Correlations in doped antiferromagnets

Moshe Havilio* and Assa Auerbach†
Department of Physics, Technion, Haifa 32000, Israel
(Received 3 January 2000)

A comprehensive study of doped resonating valence bond states is performed. It reveals a fundamental connection between superconductivity and quantum spin fluctuations in underdoped cuprates: *Cooper pair hopping* strongly reduces the local magnetization m_0. This effect pertains to recent muon spin rotation measurements in which m_0 varies weakly with hole doping in the poorly conducting regime, but drops precipitously above the onset of superconductivity. The Gutzwiller mean field approximation (GA) is found to agree with numerical Monte Carlo calculations. The GA shows, for example, that for a bond amplitude $u(r) = e^{-r/\xi}$, spin-spin correlations decay exponentially with a correlation length $\propto e^{3\pi\xi^2/2}$. The expectation value of the Heisenberg model is found to be correlated with the average loop density.

I. INTRODUCTION

When holes are introduced into the copper oxide planes of high-T_c cuprates, spin and charge correlations change dramatically. The *local* magnetization m_0, measured by muon spin rotation[1] (μSR) on, e.g., $La_{2-x}Sr_xCuO_4$, reveals a qualitative difference between the insulating and superconducting phases: m_0 is rather insensitive to doping in the poorly conducting regime $0 \leqslant x \leqslant 0.06$, but drops precipitously above the onset of superconductivity at $x > 0.06$, becoming undetectable at optimal doping $x \approx 0.15$. Theoretically, holes can cause *dilution* and *frustration* in the Heisenberg antiferromagnet, which create spin textures: either random (''spin glass'') or with ordering wave vector away from (π, π) (sometimes called ''stripes'').[3] However, the apparent reduction of local magnetization by the onset of superconductivity is a novel and poorly understood effect. Theory must go beyond purely magnetic models, and involve the superconducting degrees of freedom.

We find that this problem is amenable to a variational approach, using hole-doped resonating valence bond (RVB) states.[4] The RVB states were originally suggested by Anderson to describe the spin and charge correlations in the high-T_c cuprates.[5] They are excellent trial wave functions for the doped Mott insulators, with large Hubbard repulsion U since (i) configurations with doubly occupied sites are excluded and (ii) Marshall's sign criterion for the magnetic energy[6] is satisfied, and the Heisenberg ground state energy and antiferromagnetism at zero doping is accurately recovered.[7,8]

The hole-doped RVB state is a new class of variational states, in which spin and charge correlations are parametrized independently, without explicit spin or gauge symmetry breaking. Such parametrization allows states with magnetic and independently *d* or *s* wave superconducting (off-diagonal) order or disorder, thus permitting an *unbiased* determination of ground-state spin and charge correlations appropriate for the cuprates. These are important advantages over commonly used spin-density-wave, Hartree-Fock, and BCS wave functions.

A comprehensive study of the state is performed using Monte Carlo and mean field calculations. A phenomenological low-energy effective Hamiltonian is proposed, with two major components: Heisenberg interaction for spins and single or Cooper pair hopping kinetic energy for fermion holes.

Regarding this model our key results are the following.

(i) For the magnetic energy alone, the local magnetization m_0 is *weakly dependent* on doping concentration. This holds independently of interhole correlations for either randomly localized or extended states.

(ii) In contrast to (i), m_0 is strongly reduced by the kinetic energy of *Cooper pair hopping*, which correlates the reduction of m_0 with the rise of superconducting stiffness and, hence,[9] the transition temperature T_c.

These results agree with the experimentally reported correlation between m_0 and T_c.[1] This relation appears to be *weakly* dependent on the precise hole density.

We also find that RVB states have the following properties.

(i) The magnetic energy is correlated with the average loop density: $\Gamma = L^2 m_0^2/(\text{average radius of gyration of a loop})^2$, where L is the linear size off the lattice.

(ii) The Gutzwiller mean field approximation (GA) for magnetic correlations is in good agreement with the Monte Carlo results.

(iii) Long-range magnetic correlations in RVB states are extremely sensitive to changes in the singlet bond amplitude u. For example, with $u(r) = \exp(-r/\xi)$ the spin-spin correlation function decays exponentially with correlation length $\xi_{ex} \propto \exp[(1-x)(3\pi/2)\xi^2]$, where x is the hole concentration.

The paper is organized as followed: Section II introduces the hole-doped RVB state, and discusses the numerical procedure. Section III defines our variational parameters. Section IV deals with the antiferromagnetic and superconducting order parameters. Section V deals with the components of the effective Hamiltonian. Section VI correlates between superconducting T_c and local magnetization. Section VII is a summary and discussion.

The paper has three appendixes. Appendix A reduces the hole part of the doped RVB to a numerically convenient format. Appendix B derives expressions for expectation values. Particularly, an alternative procedure to calculate the

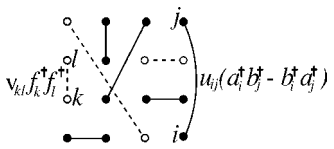

FIG. 1. A bond configuration in the doped RVB states $\Psi[u,v]$. Solid (open) circles represent spins (holes) with bond correlations $u_{ij}\,(v_{kl})$.

magnetic correlation is derived and used to check the computer program. In Appendix C, the GA is performed analytically.

II. HOLE-DOPED RESONATING VALENCE BOND STATES

A valence bond (VB) state is

$$|\alpha\rangle = \prod_{(i,j)\in\alpha} (a_i^\dagger b_j^\dagger - b_i^\dagger a_j^\dagger)|0\rangle, \tag{1}$$

where α is a pair covering of the lattice, $a_i^\dagger, b_j^\dagger$ are Schwinger bosons, and $i=1,\ldots,L^2$ is a site index on a square lattice.

RVB states are superposition of VB states. We restrict the disscussion to

$$|\Psi[u]\rangle = \sum_\alpha \prod_{(i,j)\in\alpha} u_{ij}(a_i^\dagger b_j^\dagger - b_i^\dagger a_j^\dagger)|0\rangle, \tag{2}$$

where $u(\mathbf{r}_{ij})\geqslant 0$ is a variational singlet bond amplitude, which connects sites of different sublattices A and B only. This ensures Marshall's sign.[6]

The hole-doped RVB state is defined by

$$|\Psi[u,v;x]\rangle = \mathcal{P}_G(x)|\overline{\psi}[u,v]\rangle$$
$$|\overline{\psi}[u,v]\rangle \equiv \exp\left[\sum_{i\in A, j\in B} [v_{ij} f_i^\dagger f_j^\dagger + u_{ij}(a_i^\dagger b_j^\dagger - b_i^\dagger a_j^\dagger)]\right]|0\rangle, \tag{3}$$

where $f_i^\dagger$ are spinless hole fermions, $u_{ij}\geqslant 0$, and $v(\mathbf{r}_{ij})$ is an *independent* hole bond parameter. The Gutzwiller projector $\mathcal{P}_G(x)$ imposes two constraints: a constraint of no double occupancy

$$n_a^i + n_b^i + n_f^i = 1 \quad \forall i, \tag{4}$$

and a global constraint on the total number of holes,

$$\sum_i n_f^i = xL^2 = N_h. \tag{5}$$

Due to $\mathcal{P}_G(x)$, Ψ can be written as a sum over bond configurations of singlets and hole pairs which cover the lattice as depicted in Fig. 1.

An overlap of two VB states, $\langle\alpha|\beta\rangle$, is expressed in terms of a directed loop covering of the lattice (DLC),[7,10,15] and hence

$$\langle\Psi[u]|\Psi[u]\rangle = \sum_\Lambda \Omega_\Lambda, \tag{6}$$

where Λ is a DLC,

$$\Omega_\Lambda \equiv \prod_{\lambda\in\Lambda} \left(2 \prod_{(i,j)\in\lambda} u_{ij}\right), \tag{7}$$

and λ is a directed loop.

With the results of Appendix A, the norm of the doped RVB state is

$$\langle\Psi[u,v;x]|\Psi[u,v;x]\rangle = \sum_{\gamma,\Lambda(\gamma)} W(\gamma,\Lambda(\gamma)), \tag{8}$$

where γ is a *distinct* configuration of N_h holes sites:

$$\gamma \equiv \{(i_k\in A, j_k\in B)\}_{k=1}^{N_h/2}: \quad \forall k<k' \; i_k<i_{k'}, \quad j_k<j_{k'},$$

Λ_γ is a DLC which coveres the lattice but the hole sites,

$$W(\gamma,\Lambda_\gamma) = \begin{cases} \det^2 V(\gamma)\Omega_{\Lambda_\gamma}, & x>0, \\ \Omega_\Lambda, & x=0, \end{cases} \tag{9}$$

and V is an $N_h/2\times N_h/2$ matrix with

$$V(\gamma)_{kl} \equiv v_{i_k j_l}. \tag{10}$$

Expectation value of an operator O is expressed as a weighted sum

$$\langle O\rangle = \frac{1}{\langle\Psi|\Psi\rangle} \sum_{\gamma,\Lambda_\gamma} W(\gamma,\Lambda_\gamma) O(\gamma,\Lambda_\gamma) \equiv \overline{O}, \tag{11}$$

where $O(\gamma,\Lambda_\gamma)$ is defined by Eqs. (9) and (11).

We use standard Metropolis algorithm[11] for the evaluation of sum (11). The basic Monte Carlo step for updating the DLCs is the one used by Ref. 7: Choose at random a site and one of its next-nearest neighbors and exchange, with transition probability that satisfies detailed balance, the bonds connecting each of them, either to the next site (forward bond) or the previous site in their loops. In Ref. 12 we show, that for $u_r>0\;\forall r$, these steps are *ergodic*; that is, any DLC can be reached from any other by a sequence of Monte Carlo steps.

For the fermion holes our update scheme is a simple generalization of the ''inverse-update'' algorithm of Ceperley, Chester, and Kalos.[13] According to Eq. (10), changing a position of an $A\,(B)$ sublattice hole amounts to changing one row (column) in the matrix V. In our calculation boundary conditions are periodic.

For the dimer-doped RVB state, where

$$u_{ij} = v_{ij} = \begin{cases} 1, & |\mathbf{r}_{ij}| = 1, \\ 0, & \text{otherwise}, \end{cases} \tag{12}$$

we obtained exact results using the transfer matrix technique. For a 4×40 undoped lattice[14] the magnetic energy is $E_{mag} = -0.320\,744J$/bond. The Monte Carlo result is -0.3210 ± 0.0002. $\langle \mathbf{S}_0\mathbf{S}_r\rangle$ is exponentially decaying with correlation length of $\xi_{\text{dimer}} = 0.724$; the Monte Carlo result is 0.738. Exact and Monte Carlo results for the doped 2×64 ladder[12]

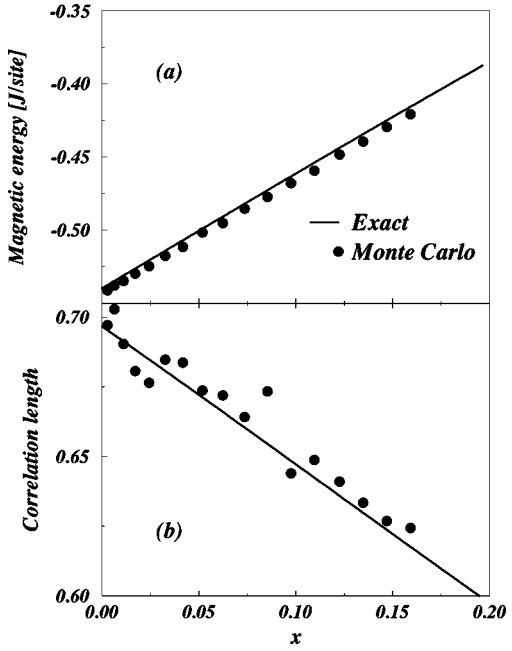

FIG. 2. Exact and numerical Monte Carlo results of magnetic energy and correlation length of the spin-spin correlation function vs hole doping x (Ref. 12). Dimers v and u, Eq. (12), are used on a 2×64 ladder.

appear in Fig. 2. Our program successfully reproduced existing data for RVB states.[7,8,12] Other tests of the program appear below.

We also use the GA to evaluate expectation values in the doped RVB state. The GA is discussed in Appendix C.

III. VARIATIONAL PARAMETERS

In the undoped, $x=0$, case we treat three classes of the singlet bond amplitude u:

$$u_p(r)=\frac{1}{r^p}, \tag{13}$$

$$u_{ex}(r)=u_{sr}(r)\frac{1}{r^{0.4}}\exp\left(-\frac{r}{\xi}\right), \tag{14}$$

$$u_g(r)=u_{sr}(r)\exp(-Qr^2), \tag{15}$$

with $u(1)=1$ and

$$u_{sr}(r)=a_1\exp\left(-\frac{r}{\xi_{sr}}\right)+a_2, \tag{16}$$

where, for u_{ex} (u_g), $\xi_{sr}^{-1}=1.7(2)$ and $a_2=0.05$ (0.018). Here u_{sr} determines the short-range decay of u_{ex} and u_g.[12] We also use $u=u_{MF}$. Here u_{MF} is derived from the Schwinger-boson mean field theory of the Heisenberg model.[15,8] For $x>0$ we use u_p, Eq. (13), and u_{ex}, Eq. (14).

For the function v the following cases of interhole correlations are treated:

$$v_{ins}^{\gamma}(\mathbf{r}_{ij})=\begin{cases}1, & (i,j)\in\gamma,\\ 0, & (i,j)\notin\gamma,\end{cases}$$

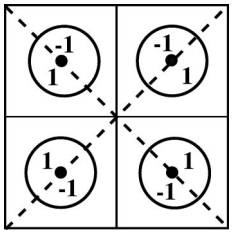

FIG. 3. $v=v_{\mathbf{k}}^{met}$. Σ is centered at Fermi pockets around $\mathbf{k}_{min}=(\pm\pi/2,\pm\pi/2)$. Within the pockets $v_{met}=\pm 1$; otherwise $v_{met}=0$. Note that v_{met} has $d_{x^2-y^2}$ symmetry.

$$v_{\mathbf{r}}^{met}=\frac{1}{L^2}\sum_{\mathbf{k}\in\Sigma} v_{\mathbf{k}}^{met}e^{-i\mathbf{k}\cdot\mathbf{r}},$$

$$v_{\alpha}(\mathbf{r})=\sum_{\hat{\eta}} c_{\alpha}(\hat{\eta})\delta_{\mathbf{r},\hat{\eta}}, \quad \alpha=s,d, \tag{17}$$

where $|v_{\mathbf{k}}^{met}|=1$, $\hat{\eta}$ are nearest-neighbor vectors on the square lattice, $c_s=1$, and $c_d=\hat{\eta}_x^2-\hat{\eta}_y^2$.

v_{ins}^{γ} puts the N_h holes on random sites. This state describes an insulator with disordered localized charges.

v_{met} describes weakly interacting holes in a ''metallic'' state:

$$\prod_{\mathbf{k}\in\Sigma} f_{\mathbf{k}}^{\dagger}|0\rangle=\mathcal{P}_G(x)\exp\left(\sum_{\mathbf{k}} v_{\mathbf{k}}^{met}f_{\mathbf{k}}^{\dagger}f_{-\mathbf{k}+(\pi,\pi)}^{\dagger}\right)|0\rangle$$

$$=\mathcal{P}_G(x)\exp\left(\sum_{ij} v_{ij}^{met}f_i^{\dagger}f_j^{\dagger}\right)|0\rangle, \tag{18}$$

where the product is over N_h states,

$$v_{\mathbf{k}}^{met}=\begin{cases}\mathrm{sgn}(\mathbf{k}), & \mathbf{k}\in\Sigma,\\ 0, & \mathbf{k}\notin\Sigma,\end{cases} \tag{19}$$

and $v_{ij}^{met}=\Sigma_{\mathbf{k}}v_{\mathbf{k}}^{met}e^{-i\mathbf{k}(\mathbf{r}_i-\mathbf{r}_j)}$. Here we check Σ which is centered at $\mathbf{k}_{min}=(\pm\pi/2,\pm\pi/2)$. See Fig. 3. Results for Σ centered at $\mathbf{k}_{min}=(0,\pm\pi)$, $(\pm\pi,0)$ are *not* qualitatively different.[12] v_{met} obey

$$v_{\mathbf{k}+(\pi,\pi)}=-v_{\mathbf{k}}; \tag{20}$$

hence v_{ij}^{met} only connects $i\in A$ to $j\in B$. Correlations in a state with $v=v_{met}$ were previously computed by Bonesteel and Wilkins.[16]

v_s and v_d describe tightly bound hole pairs in relative s- and d-wave symmetry, respectively.

IV. ORDER PARAMETERS

A. Local magnetic moment and long-range magnetic correlations

The local magnetization is

$$m_0^2=\frac{1}{L^4}\sum_{ij}\langle\mathbf{S}_i\cdot\mathbf{S}_j\rangle e^{-i(\pi,\pi)(\mathbf{r}_i-\mathbf{r}_j)}, \tag{21}$$

where, e.g., $S^+=S^x+iS^y\equiv a^{\dagger}b$. With respect to Eq. (11), $\langle\mathbf{S}_i\cdot\mathbf{S}_j\rangle\equiv S(r_{ij})$ is calculated using[7]

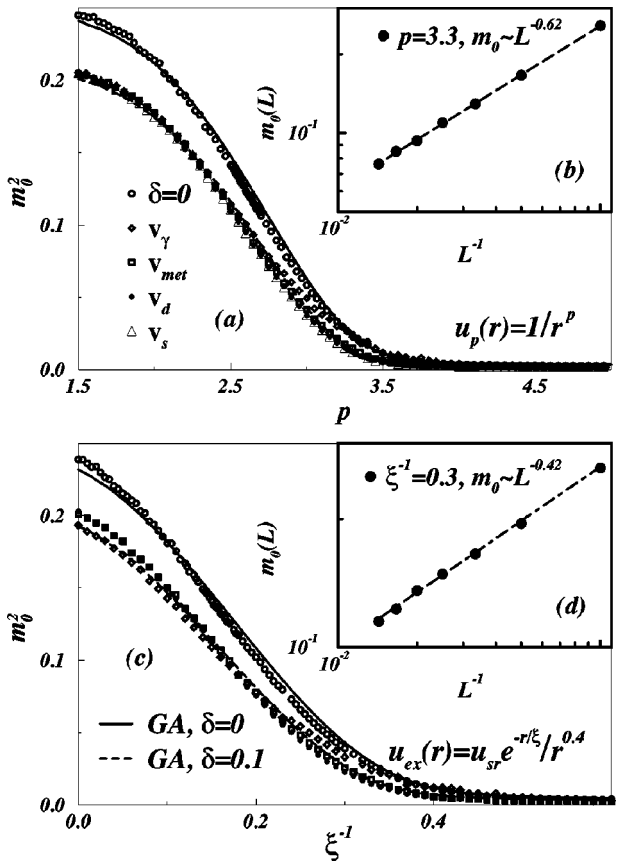

FIG. 4. (a) The local magnetization squared, $m_0^2(p)$, of doped and undoped RVB wave functions vs the variational power p, defined by Eq. (13). The lattice size is 40×40, and in the doped case the hole concentration is 10%. Results agree with the Gutzwiller approximation (lines). The hole bond parameters v are defined in Eq. (17). m_0^2 is weakly dependent on v. (b) Finite-size scaling of $m_0(L)$ for $p=3.3$ which indicates vanishing local magnetization at $L\to\infty$. (c) $m_0^2(\xi)$ vs the variational correlation length ξ, defined by Eq. (14). (d) Finite-size scaling of $m_0(L)$ for $\xi^{-1}=0.3$ which indicates vanishing local magnetization at $L\to\infty$.

$$\mathbf{S}_i\cdot\mathbf{S}_j(\gamma,\Lambda_\gamma)_1=\begin{cases}\pm\frac{3}{4}, & ij \text{ are on the same loop in } \Lambda_\gamma,\\ 0, & \text{otherwise,}\end{cases} \tag{22}$$

where the sign is $+$ if i and j are on the same sublattice. To check our program we also used an alternative procedure to calculate magnetic cerrelations. See Appendix B 1.

In Fig. 4(a), $m_0^2(p)$ is plotted for $\Psi[u_p;x=0]$ and $\Psi[u_p,v;x=0.1]$ for various choices of v. Finite-size scaling in Fig. 4(b) for $x=0.1$ indicates vanishing long-range order, $m_0\to0$, at $p_c=3.3$. It lowers the bound given previously by Ref. 7: at $p_c\leqslant5$. In Fig. 4(c), $m_0^2(\xi^{-1})$ is plotted for $\Psi[u_{ex};x=0]$ and $\Psi[u_{ex},v;x=0.1]$. Finite-size scaling in Fig. 4(d) indicates $m_0\to0$, at $\xi^{-1}=0.3$. In all the cases the GA (lines) works well.

Good agreement between GA and Monte Carlo is also seen in Figs. 5(a) and 5(b), where $S(r)$ is plotted for u_p, and u_{ex}, respectively. Note how slow $S(r)$ decays for $\xi^{-1}=0.3$. By Fig. 4(b), $m_0(L)\sim L^{-0.42}$ in this state. Exponentially decaying spin correlations are seen, both by Monte Carlo simulations and the GA, for u_p with $p\gtrsim3.7$ and u_{ex} with $\xi^{-1}\gtrsim0.4$.[12] Details of u_{sr}, Eq. (16), have a strong effect on long-range spin correlations.

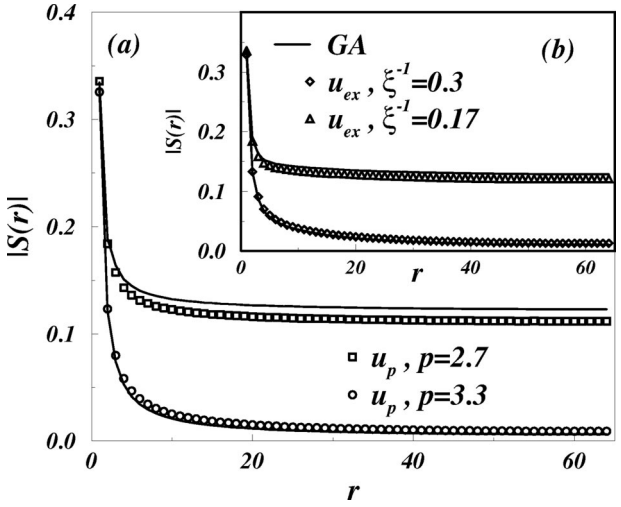

FIG. 5. (a) Calculations of the spin-spin correlation function $[S(r)]$ with Monte Carlo simulations and the GA (lines) for undoped states with $u=u_p$, Eq. (13). The size of the lattice is $L=128$. (b) Calculations of $S(r)$ using $u=u_{ex}$, Eq. (14). Note how slow $S(r)$ decays. In both cases there is a good agreement between Monte Carlo and GA, and $S(r)$ weakly effected by doping.

We use the GA to extrapolate Monte Carlo calculations for $S(r)$. In Appendix C1 we find for the exponential bond amplitude $u(r)=\exp(-r/\xi)$ and $\xi\gg1$ that $S(r)$ decays exponentially with correlation length:

$$\xi_{ex}\propto\exp\left((1-x)\frac{3\pi}{2}\xi^2\right). \tag{23}$$

For the Gaussian bond amplitude $u(r)=\exp(-\mu r^2)$ with $\mu\ll1$, we find in Appendix C2 that $S(r)$ decays exponentially with correlation length:

$$\xi_g\propto\frac{1}{\sqrt{\mu}}\exp\left((1-x)\frac{\pi}{4\mu}\right). \tag{24}$$

For u_p, Appendix C 3 suggests vanishing long-range order, $m_0\to0$, at $p_c\leqslant3$.

The correlation lengths (23) and (24) explain the slow decay of $S(r)$ in Fig. 5(b). It also indicates that in the $L=\infty$ system, a small change in the ground-state parameters brings an extremely sharp change in long range magnetic correlations.

B. Superconducting order parameter

The superconducting singlet order parameters are

$$\Delta_i^{s,d}=\sum_{\hat{\eta}}c_{s,d}(\hat{\eta}), \tag{25}$$

where

$$\Delta_{ij}=f_i^\dagger f_j^\dagger(a_ib_j-b_ia_j)/\sqrt{2}. \tag{26}$$

The expressions of Δ matrix elements are discussed in Appendix B3. By gauge invariance imposed by the Gutzwiller

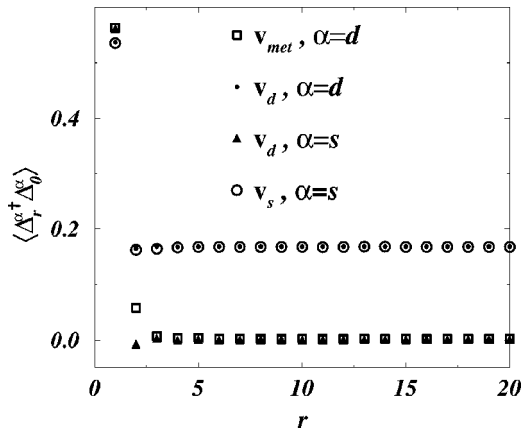

FIG. 6. The singlet pair correlation function. $\langle(\Delta_r^\alpha)^\dagger\Delta_0^\alpha\rangle$. Δ_i^α is defined in Eq. (25), and $\alpha=s,d$. In this graph $u=1/r^{3.3}$. $\Psi[u,v_\alpha;x]$ has superconducting (off-diagonal) long-range order (ODLRO) only of symmetry α. $\Psi[u,v_{met};x]$ has no ODLRO in either symmetry.

projector, $\langle\Delta^{s,d}\rangle=0$. However, $\Psi[u,v_{s(d)};x>0]$ describes true s-(d-) wave superconductors as seen by the singlet pair correlation function $\langle(\Delta_r^\alpha)^\dagger\Delta_0^\alpha\rangle$, $\alpha=s,d$, in Fig. 6. For $v=v_\alpha$, $\lim_{r\to\infty}\langle(\Delta_r^\alpha)^\dagger\Delta_0^\alpha\rangle\neq 0$, and Ψ has (off-diagonal) long-range order in Δ_α. In contrast, the insulator states $\Psi[u,v_{ins},x]$ and the ''metallic'' states $\Psi[u,v_{met},x]$ have no long-range superconducting order of either symmetry.

V. EFFECTIVE HAMILTONIANS

A. Magnetic energy and related parameters

Magnetic order is driven by the diluted antiferromagnetic quantum Heisenberg model

$$\mathcal{H}^J=J\sum_{\langle ij\rangle}\mathbf{S}_i\cdot\mathbf{S}_j. \tag{27}$$

Magnetic energy for $x=0$: In Fig. 7(a), $E_{mag}(p)$, $E_{mag}(\xi)$, and $E_{mag}(Q)$ are plotted as a function of $m_0^2(p)$, $m_0^2(\xi)$, and $m_0^2(Q)$ for u_{ex}, u_p, and u_g, Eqs. (13), (14), and (15), respectively. In $x=0$, *all* the three bond amplitudes yield a lowest magnetic energy of

$$E_0=-0.335\pm 0.0005J/\text{bond}, \tag{28}$$

For u_p, the optimal value of p is $p_{optimal}=2.7$, and $m_0^2(p=2.7)=0.105\pm 0.005$. The ground-state parameters of the Heisenberg model on an $L=40$ lattice are $E(\text{ground state})=0.3347J/\text{bond}$ and $m_0^2(\text{ground state})=0.109$.[17] Table I contains a summary of results for the optimal choice of parameters in all the classes.

Magnetic energy for $x=0.1$: In Fig. 8, $E_{mag}(p)$ and $E_{mag}(\xi)$ are plotted as a function of $m_0^2(p)$ and $m_0^2(\xi)$, for $x=0.1$ and various choices of v from Eq. (17). Within numerical errors, all states minimize $\mathcal{H}^J$ at the same optimal parameters as for $x=0$ (Table I). For u_p, by Fig. 4(a) it yields a local magnetization of $m_p^2(x=0.1)=0.08$. For u_{ex}, Fig. 4(c) shows $m^2(x=0.1)=0.1$. Thus we conclude that

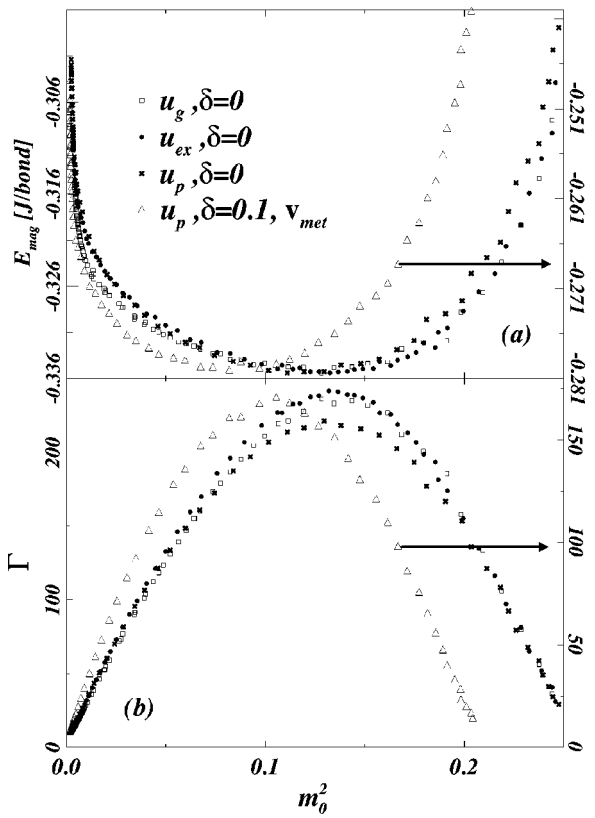

FIG. 7. (a) Magnetic energy (E_{mag}) vs local magnetization squared m_0^2. Variational parameters are for $x=0$ (left y scale), $u_p(p)$, Eq. (13), $u_{ex}(\xi)$, Eq. (14), and $u_g(Q)$, Eq. (15). For $x=0.1$ (right y scale) v_{met} and u_p. lattice size is $L=40$. The optimal parameters for each u appear in Table I. The minimal magnetic energy for $x=0$ is $-0.335\pm 0.0005J/\text{bond}$. (b) The average density of a loop per site Γ, Eq. (32), vs m_0^2 for variational cases as in (a). In all the cases Γ is correlated with E_{mag}.

aside from the trivial kinematical constraints, *the hole density and correlations have little effect on the magnetic energy at low doping.*

A better understanding of the properties of the optimal bond amplitude for $\mathcal{H}^J$ is gained by the *average loop density* defined below. From Eq. (22), a DLC contributes to m_0^2, Eq. (21), its number of pairs of sites, which share the same loop, hence

$$m_0^2=\frac{3}{4L^4}\overline{\left(\sum_{\lambda\in\Lambda_\gamma}l_\lambda^2\right)}=\frac{3}{4L^4}\overline{\left(\sum_{i\notin\gamma}l_{\lambda_i}\right)}, \tag{29}$$

TABLE I. Minimal magnetic energy (E_0), optimal choice of parameters, and square of the ground-state magnetization (m_0^2), for various bond amplitudes in the undoped, $x=0$, case. The size of the lattice is $L=40$. u_{MF} is derived from the Schwinger-boson mean field theory of $\mathcal{H}^J$. The ground-state parameters of the Heisenberg model on an $L=40$ lattice are $E(\text{ground state})=0.3347J/\text{bond}$ and $m_0^2(\text{ground state})=0.109$ (Ref. 17).

state	$E_0(x=0)[J/\text{bond}]$	E_0 parameters	$m_0^2(x=0)$
u_{ex}, Eq. (14)	-0.335 ± 0.0005	$\xi^{-1}=0.17\pm 0.005$	0.125 ± 0.005
u_g, Eq. (15)	-0.335 ± 0.0005	$Q=0.014\pm 0.001$	0.12 ± 0.005
u_p, Eq. (13)	-0.335 ± 0.0005	$p=2.7\pm 0.05$	0.105 ± 0.005
u_{MF}	-0.3344 ± 0.0002		0.087 ± 0.005

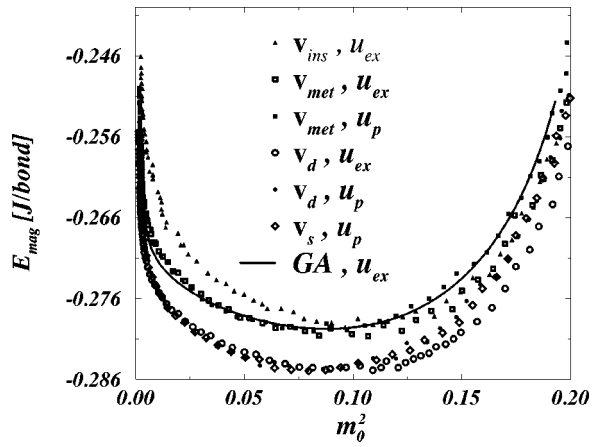

FIG. 8. Magnetic energy (E_{mag}), for u_p Eq. (13), and u_{ex} Eq. (14), vs local magnetization squared m_0^2, using various hole distributions from Eq. (17). The density of holes is $x=0.1$ and lattice size is $L=40$. E_{mag} is weakly dependent on interhole correlations. For u_p (u_{ex}), E_{mag} is minimized at $m_0^2(p)\approx 0.08(0.1), p=2.7(\xi^{-1}=0.17)$.

where $l_\lambda=\Sigma_{i\in\lambda}1$ is the loop length, and $i\in\lambda_i$. Thus $L^2m_0^2=S(\pi,\pi)$ is proportional to the average loop length per site.

The average radius of gyration of a loop is

$$r_g\equiv\overline{\left(\frac{1}{n_\Lambda}\sum_{\lambda\in\Lambda_\gamma} r_g^\lambda\right)}, \tag{30}$$

where

$$(r_g^\lambda)^2=\frac{1}{l_\lambda}\sum_{i\in\lambda}(\mathbf{r}_i-\mathbf{r}_{\text{c.m.}}^\lambda)^2=\frac{1}{2l_\lambda^2}\sum_{i,j\in\lambda}(\mathbf{r}_i-\mathbf{r}_j)^2, \tag{31}$$

with $r_{\text{c.m.}}^\lambda=(1/l_\lambda)\Sigma_{i\in\lambda}\mathbf{r}_i$, and n_Λ is the number of loops in the DLC Λ. With Eqs. (29) and (30) we define the average density of a loop per site:

$$\Gamma\equiv\frac{L^2m_0^2}{r_g^2}. \tag{32}$$

The average loop density Γ is plotted in Fig. 7(b), in the undoped case for all the bond amplitudes (13), (14), and (15); and in the doped case for $\Psi[u_p,v_{met};x=0.1]$. Comparison with Fig. 7(a) shows that Γ is correlated with the magnetic energy. For vanishing m_0, Γ converges to its value in the dimer RVB state, Eq. (12), where $\Gamma(\text{dimer RVB})\approx 9.6$. This value of Γ is only slightly larger than that of an ensemble of DLCs, which include only configurations with two- (or four-) site loops with dimer bonds. For such loops $r_g^\lambda=0.5$ (or $\sqrt{2}/2$) and $\Gamma=l_\lambda/r_{g,\lambda}^2=8$.

The occurrence of loop lengths (l_λ) is interesting. In Fig. 9 we plot an histogram of the number of loops ($\overline{n_\lambda}$) versus the number of sites on a loop (l_λ). The size of the lattice is $L=128$, and $u=u_{MF}$, which is derived from the Schwinger-boson mean field theory of $\mathcal{H}^J$.[15] For all the bond amplitudes and lattice sizes we have checked $\overline{n_\lambda}(l)$ decays either algebraically or exponentially.

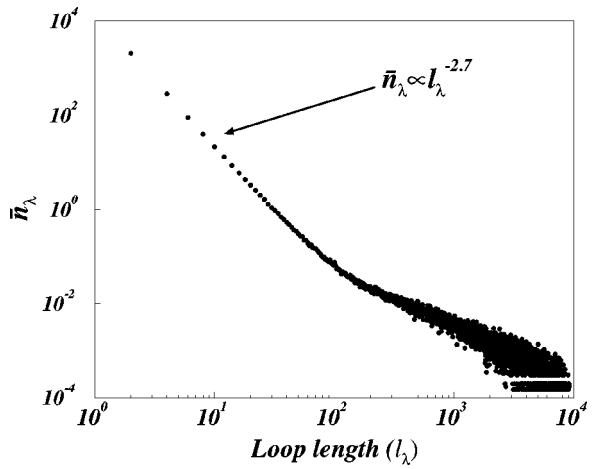

FIG. 9. The average number of loops ($\overline{n_\lambda}$) vs the number of sites on a loop (l_λ). The state is with $u=u_{MF}$, which is derived from the Schwinger-boson mean field theory of $\mathcal{H}^J$. The size of the lattice is $L=128$. For $l_\lambda\lesssim 130$, $n_l\propto l_\lambda^{-2.7}$.

B. Single-hole hopping energy

A single-hole hopping in the antiferromagnetic (AFM) background has been shown by semiclassical arguments[18,15] to be effectively restricted at low energies to hopping between sites on the same sublattice:

$$\mathcal{H}^{t'}=\sum_{\langle ik\rangle\in A,B} t'_{ik}f_i^\dagger f_k(a_k^\dagger a_i+b_k^\dagger b_i), \tag{33}$$

where i,k are removed by two adjacent lattice steps, and $t'>0$. Unconstrained, the single-hole ground state of $H^{t'}$ has momentum on the edge of the magnetic Brillouin zone, in agreement with exact diagonalization of t-J clusters.[19] Previous investigations have found that *intersublattice* hopping (the t term in the t-J model) is a high-energy process in the AFM correlated state.[18,15] We thus expect the same to hold even in RVB spin liquids with strong short-range AFM correlations but no long-range order. The primary effects at low doping may be to shift the ordering wave vector.

We denote by t'_d (t'_h) the coefficients of second (third) nearest-neighbor hopping terms. For $t'_h>t'_d/2$ the single-hole bend minimum is at $\mathbf{k}_{min}=(\pm\pi/2,\pm\pi/2)$; otherwise $\mathbf{k}_{min}=\pm(0,\pi),\pm(\pi,0)$. Here we put $t'_h=1$, $t'_d=0.5$.

Results for the expectation value of $H^{t'}$ are plotted in Fig. 10. The single-hole hopping, Eq. (33), prefers the metallic states $v=v_{met}$ over states with $v=v_s,v_d$.[12] It also prefers longer-range $u(r)$ and thus actually *enhances* magnetic order at low doping. This is a type of a Nagaoka effect, where mobile holes separately polarize each of the sublattices ferromagnetically.

C. Double-hopping energy

We consider Cooper pairs hopping terms

$$\mathcal{H}^{J'}=-J'\left(\sum_{ijk}\Delta_{ij}^\dagger\Delta_{ik}+\sum_{\langle ij\rangle,i'j'}\Delta_{ij}^\dagger\Delta_{i'j'}\right). \tag{34}$$

Calculation of $\mathcal{H}^{J'}$ matrix elements is discussed in Appendix B3. The first term in $\mathcal{H}^{J'}$ is derived from the large U Hub-

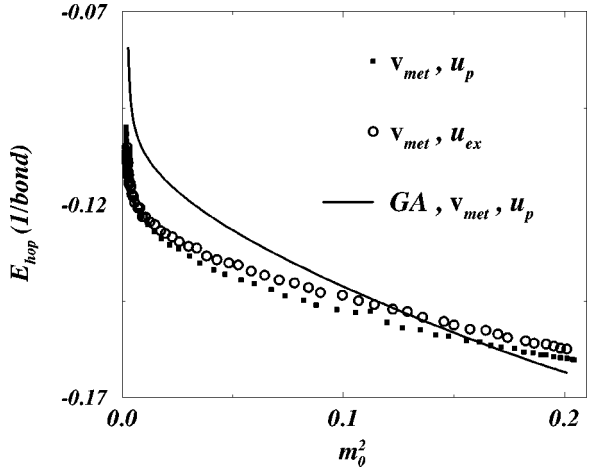

FIG. 10. The single-hole hoping energy E_{hop}, Eq. (33), vs local magnetization squared m_0^2 for metalic hole distributions, and spin bond amplitudes u_p and u_{ex}. The density of holes is $x=0.1$ and lattice size is $L=40$. In $H^{t'}$, $t_h'=1$, $t_d'=0.5$, and the single-hole band minimum is at $\mathbf{k}_{min}=(\pm\pi/2,\pm\pi/2)$. The single-hole hopping prefers longer-range $u(r)$ and hence higher local magnetic moment. It also pefers metallic states over $v=v_s, v_d$ (Ref. 12).

bard model to order $J'=t^2/U$.[15] It includes terms (a) and (b) in Fig. 11. Term (a) is a *rotation* of the singlet pair. It is positive for v_s (Ref. 12) and hence prefers v_d over v_s. Term (c) in Fig. 11 is a parallel *translation* of singlets. It prefers superconductivity with $v=v_d$ or $v=v_s$ over metallic states with $v=v_{met}$.[20] For $x=0.1$, $\mathcal{H}^{J'}$ is minimized by v_d.

In Fig. 12 the ground-state energy E_{ph} of Eq. (34) is plotted for $v=v_d$, $u=u_p$, and $u=u_{ex}$. Here $x=0.1$, and the size of the lattice is $L=40$. The variational energy is minimized at $p=3.35$ and $\xi^{-1}=0.35$, for u_{ex} and u_p, respectively. In both cases, by the finite-size scaling of Figs. 4(b) and 4(d), it indicates vanishing m_0 at $L\to\infty$. *Thus, Cooper pair hopping drives the ground state toward a spin liquid phase.*

The Gutzwiller approximation fails to predict this effect. According to the GA, the minimum of the double-hopping energy roughly coincides with the minimum of the magnetic energy ($\langle\mathcal{H}^J\rangle$). This is understood by (see Appendix C)

$$\langle S_i^+ S_j^-\rangle_{GA}=-\langle a_i^\dagger b_j^\dagger\rangle_{GA}^2,$$

where $i\in A$, $j\in B$. The GA agrees with Monte Carlo results for matrix elements of *long-range* pair hopping.

The matrix element of (d) in Fig. 11 and $\langle n_i^f n_j^f\rangle$ also drives the ground state toward a spin liquid, and prefers superconducting over metallic states.[12] These terms are excluded due to relatively large thermal noise.

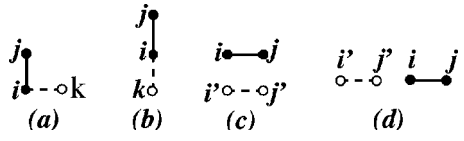

FIG. 11. (a), (b), and (c) are the terms of $H^{J'}$, Eq. (34). Dashed line and open circles = Δ. Term (a) is a rotation of a singlet pair; it distinguishes between s- to d-wave superconducting order parameters. The term (c) prefers $v_{d(s)}$ over metallic states with v_{met}. Term (d) dependence on the variational parameters is similar to that of (c); it is excluded due to thermal noise.

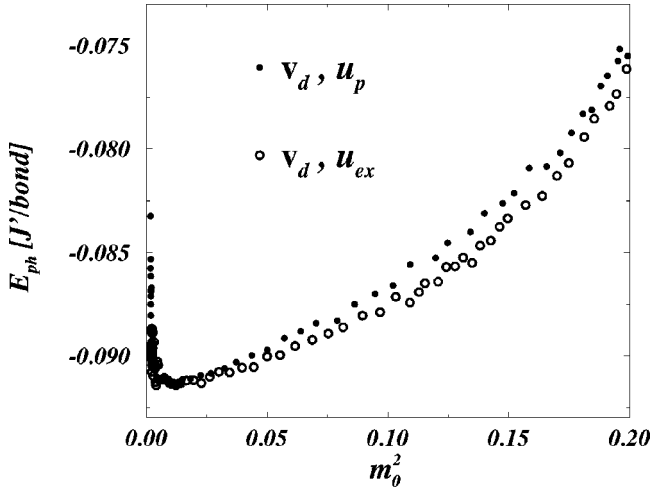

FIG. 12. The expectation value of $H^{J'}$, Eq. (34), E_{ph}, vs m_0^2, for u_p and u_{ex}. In contrast to the magnetic energy, Fig. 8, E_{ph} prefers a *vanishing* m_0 at $L\to\infty$. Note how similar the graphs are for u_{ex} and u_p.

VI. RELATION BETWEEN SUPERCONDUCTING T_c AND LOCAL MAGNETIZATION

Since $\mathcal{H}^{J'}$ is the effective model which drives superconductivity, it produces phase stiffness, which in the continuum approximation is given by

$$\mathcal{H}^{J'}\approx\frac{V_0}{2}\int d^2x(\nabla\phi_i)^2. \tag{35}$$

The stiffness constant V_0 can be determined variationally from the doped RVB states. Imposing a uniform gauge field twist on Δ, $\Delta_{i,j}\to\Delta_{i,j}\exp[i(x_i+x_j)\phi/2L]$, $\langle\mathcal{H}^{J'}\rangle$ becomes, to second order in ϕ/L,

$$E_{ph}=\frac{V_0\phi^2}{2},$$

$$V_0=\frac{d^2E_{ph}}{d\phi^2}=2J'(\langle\Delta_{0,\hat{y}}^\dagger\Delta_{0,\hat{x}}\rangle+\langle\Delta_{0,\hat{x}}^\dagger\Delta_{0,-\hat{x}}\rangle+\langle\Delta_{0,\hat{y}}^\dagger\Delta_{\hat{x}+\hat{y},\hat{x}}\rangle). \tag{36}$$

Following Ref. 9, at low doping for the square lattice V_0 is roughly equal to T_c.

In Fig. 13 we show our main result: The staggered magnetization $m_0(p)$ for $\mathcal{H}^J+\mathcal{H}^{J'}$ is plotted against the superconducting to magnetic stiffness ratio $V_0(p)/J$ for different doping concentrations $x=0.05,0.1,0.15$, $v=v_d$, and $u=u_p$. The actual free parameter in the graph is J'/J, from which m_0 and V_0 are determined variationally. Two primary observations are made: (i) The local magnetization is sharply reduced at relatively low superconducting stiffness (and T_c/J). (ii) The relation between m_0 and V_0/J appears to be independent of x.

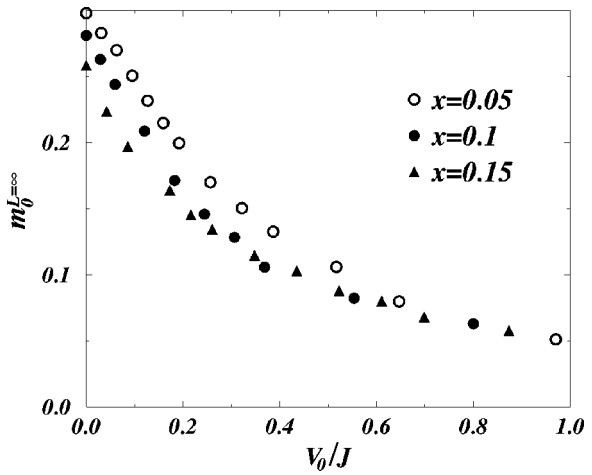

FIG. 13. The relation between thermodynamic local magnetization $m_0^{L=\infty}$ and superconducting phase stiffness V_0 (related to T_c; see text). $u=u_p$, Eq. (13). J is the Heisenberg exchange energy. The points are considered *upper bounds* on m_0, which, for u_p, may even vanish for $V_0/J \geqslant 0.2$. For u_{ex}, Eq. (14), m_0 vanishes for $V_0/J \geqslant 0.5$.

For u_{ex}, Eq. (14), it requires $V_0(\xi)/J=0.49$ for $\langle \mathcal{H}^J + \mathcal{H}^{J'} \rangle$ to be minimized at $\xi^{-1}=0.3$. By Fig. 4(b) this leads to $m_0^{L=\infty}=0$.

VII. SUMMARY AND DISCUSSION

In this paper we used extensive Monte Carlo calculations to study properties of hole-doped RVB states. We found that an effective model which includes Heisenberg and pair hopping terms is consistent with the experimental connection between superconductivity and the reduction of the local magnetic moment. Within checked variational options we showed that the properties of the model are independent of the particular choice of parameters for the state. The Gutzwiller mean field approximation for magnetic correlations was found to agree with Monte Carlo calculations, and used for analytical extrapolation of the numerical results. We showed that long-range magnetic correlations in RVB states are extremely sensitive to variational parameters. We found that the average loop density is well correlated with the magnetic energy. We conclude this paper with several arguments and insights regarding our results.

Magnetic energy and long-range magnetic correlation: Note the contrast between correlation lengths (23) and (24), and the ''shallowness'' of the minima of the magnetic energy in Fig. 8. It implies that a very weak pair hopping term in the Hamiltonian causes a dramatic change in long-range magnetic correlations.

Magnetic energy and loop density: A comparison between loops (a) and (b) in Fig. 14 shows that large amplitudes (Ω_Λ) of DLCs with ''denser'' loops enhance the probability to find nearest-neighbor sites on the same loop and reduce the magnetic energy.

The loop density shows that the optimal bond amplitude is determined by an intricate balance between m_0 and r_g. This relates *quantum spin fluctuations* to the average loop density of the ensemble.

Effective model for doped system: $\mathcal{H}^J+\mathcal{H}^{J'}$ describes the low-energy physics of the lightly doped cuprates. As the lattice is doped, its variational ground state is a *d*-wave superconductor, with a sharply reduced local magnetic moment. The model includes built-in pairing. Such a model is supported by the existence of a pseudogap in the normal state of the high T_c materials.

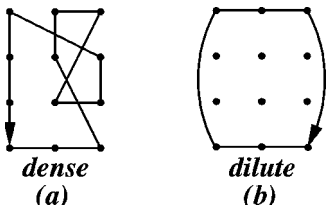

FIG. 14. Two kind of loops: (a) ''dense loops,'' which fully cover small regions of the lattice, and many nearest-neighbor pairs. Bond amplitudes u which maximize the weight (Ω_Λ) of loop configurations with such loops minimize the magnetic energy. (b) ''Dilute loops,'' which contribute very few nearest-neighbor bonds to the magnetic energy, Eq. (22). Loop (a) is denser, in the sense that it covers more sites on roughly the same ''area''$\equiv(r_g^\lambda)^2$, Eq. (31).

Relation between phase stiffness and local magnetization: Because of finite-size uncertainty, $m_0^{L=\infty}$ in Fig. 13 is an *upper* bound on the thermodynamic local magnetization. A sharper reduction of the local magnetization occurs if (a) the GA result of Appendix C3, $m_0(u_r=r^{-3})=0$, is correct to the discrete lattice. In that case m_0 vanishs already at $V_0/J \geqslant 0.2$, or (b) in finite doping the optimal bond amplitude for $\mathcal{H}^J+\mathcal{H}^{J'}$ decays exponentially. In that case m_0 vanishes for $V_0/J \gtrsim 0.5$. Variationally, we cannot rule out this possibility. In both of these cases there is a qualitative agreement with the doping dependence of the local magnetization and T_c, as measured by Refs. 2 and 1.

ACKNOWLEDGMENTS

Useful conversations with C. Henley, S. Kivelson, and S-C. Zhang, are gratefully acknowledged. M.H. thanks Taub computing center for support. A.A. is supported by the Israel Science Foundation and the Fund for Promotion of Research at Technion.

APPENDIX A: THE FERMION PART OF THE DOPPED RVB STATE

The fermion part of $|\Psi[u,v,x]\rangle$ is

$$|\Psi(x)\rangle_f = P_G(N_h)\exp\left[\sum_{i\in A, j\in B} v_{ij} f_i^\dagger f_j^\dagger\right]|0\rangle = \frac{1}{\frac{N_h}{2}!}\left[\sum_{i\in A, j\in B} v_{ij} f_i^\dagger f_j^\dagger\right]^{N_h/2}|0\rangle, \tag{A1}$$

where $N_h=xL^2$. We write this state as

$$|\Psi(x)\rangle_f \equiv \sum_\gamma C(\gamma)\prod_{k=1}^{N_h/2} f_{i_k}^\dagger f_{j_k}^\dagger|0\rangle, \tag{A2}$$

where γ is a *distinct* configuration of N_h holes sites:

$$\gamma \equiv \{(i_k \in A, j_k \in B)\}_{k=1}^{N_h/2} : \forall k < k' \; i_k < i_{k'}, \;\; j_k < j_{k'}.$$

From Eq. (A1)

$$|\Psi(N_h)\rangle_f = \frac{1}{\frac{N_h}{2}!} \sum_{\gamma} v_{\alpha_1\beta_1} \times \cdots \times v_{\alpha_{N_h/2}\beta_{N_h/2}} f^\dagger_{\alpha_1} f^\dagger_{\beta_1} \times \cdots \times f^\dagger_{\alpha_{N_h/2}} f^\dagger_{\beta_{N_h/2}} |0\rangle,$$

where $\alpha_l \in \{i_k\}_{k=1}^{N_h/2}, \beta_l \in \{j_k\}_{k=1}^{N_h/2}$. For each γ we commute *pairs* of operators, without any affect of sign, and order A holes operators in an increasing order of their site index:

$$|\Psi(N_h)\rangle_f = \sum_{\gamma} \sum_{\sigma} v_{i_1 j_{\sigma(1)}} \times \cdots \times v_{i_{N_h/2} j_{\sigma(N_h/2)}} f^\dagger_{i_1} f^\dagger_{j_{\sigma(1)}} \times \cdots \times f^\dagger_{i_{N_h/2}} f^\dagger_{j_{\sigma(N_h/2)}} |0\rangle,$$

where $\sigma = \sigma(N_h/2 \to N_h/2)$. Commuting the B operators we get

$$C(\gamma) = \det V(\gamma),$$

where V is an $N_h/2 \times N_h/2$ matrix with

$$V(\gamma)_{kl} \equiv v_{i_k j_l}.$$

When v connects same-sublattice sites the determinant is replaced by a Pffian.[12]

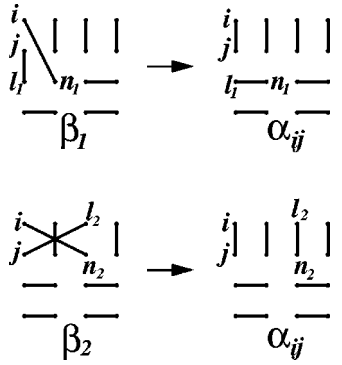

FIG. 15. According to Eq. (B4), $M^\dagger_{ij} M_{ij} |\beta_1\rangle = M^\dagger_{ij} M_{ij} |\beta_2\rangle = |\alpha_{ij}\rangle$. $M_{ij} \equiv a_i b_j - b_i a_j$.

APPENDIX B: EXPRESSIONS FOR EXPECTATION VALUES

1. Alternative calculation of magnetic correlations

We use the operator identity[15]

$$-\Delta^\dagger_{ij} \Delta_{ij} = \left[\mathbf{S}_i \cdot \mathbf{S}_j - \frac{1}{4} \right] (1 - f^\dagger_i f_i)(1 - f^\dagger_j f_j), \qquad \text{(B1)}$$

where $\Delta_{ij} = f^\dagger_i f^\dagger_j (a_i b_j - b_i a_j)/\sqrt{2}$, to express $\langle \mathbf{S}_i \cdot \mathbf{S}_j \rangle$.

We show that for $i \in A, j \in B$ and $u(r) > 0 \; \forall r$

$$\mathbf{S}_i \cdot \mathbf{S}_j(\gamma, \Lambda_\gamma)_2 - \frac{1}{4} + \frac{x}{2} = \begin{cases} -\frac{1}{2} \left(\sum\limits_{\substack{(l,n) \in \alpha \\ l \neq i}} \frac{u_{lj} u_{in}}{u_{ln} u_{ij}} + 2 \right), & (i,j) \in \alpha(\Lambda_\gamma), \\ \frac{1}{4}, & i,j \in \gamma, \\ 0, & \text{otherwise}, \end{cases} \qquad \text{(B2)}$$

where $\alpha(\Lambda_\gamma)$ is the set of forward bonds in Λ_γ, of the sites on sublattice A.

We demonstrate Eq. (B2) for a half-filled lattice ($\langle f^\dagger_i f_i \rangle = 0$). With $M_{ij} \equiv (a_i b_j - b_i a_j)$,

$$M_{ij} M^\dagger_{ij} |0\rangle = 2|0\rangle, \qquad \text{(B3)}$$

$$M_{ij} M^\dagger_{ik} M^\dagger_{mj} |0\rangle = M^\dagger_{mk} |0\rangle, \qquad \text{(B4)}$$

and hence

$$M^\dagger_{ij} M_{ij} |\Psi[u]\rangle = \sum_{\alpha_{ij}} \left[\left(\sum_{\substack{(l,n) \in \alpha_{ij} \\ l \neq i}} \frac{u_{lj} u_{in}}{u_{ln} u_{ij}} \right) + 2 \right] \times \left(\prod_{(l,n) \in \alpha_{ij}} u_{ln} \right) |\alpha_{ij}\rangle,$$

where $|\alpha_{ij}\rangle$ is a valence bond state, with $(i,j) \in \alpha_{ij}$.

The term in the square brackets requires further explanation. From Eq. (B4), for any pair $(l,n) \in \alpha_{ij} : l \neq i$, $|\alpha_{ij}\rangle = M^\dagger_{ij} M_{ij} |\beta\rangle$, where (i,j), $(l,n) \notin \beta$, (l,j), $(i,n) \in \beta$, and otherwise $\beta = \alpha$; see Fig. 15. In $|\Psi[u]\rangle$, each $|\beta\rangle$ carries a factor $u_{lj} u_{in}$. Equation (B3) indicates an additional option to get $|\alpha_{ij}\rangle$, from $|\alpha_{ij}\rangle$.

Taking the overlap with $\langle \Psi[u]|$, we get the matrix element which is expressed in terms of Eq. (B2). Here α_{ij} represents the ket. A possible definition of the bonds of the ket is the forward bonds of the sites on sublattice A.

2. Matrix element of single-hole hopping term

Figure 16 describes the effect of a single-hole hoping term on a hole-pair configuration. Using definition (11), for $i,k \in A$,

$$f_i^\dagger f_k(a_k^\dagger a_i + b_k^\dagger b_i)(\gamma,\Lambda_\gamma) = \begin{cases} \dfrac{\det V(\gamma_k)}{\det V(\gamma)} \dfrac{u_{il}}{u_{kl}} s_{ki}, & \text{if } i\in\gamma,\ k\notin\gamma, \\ 0, & \text{otherwise,} \end{cases} \tag{B5}$$

where $i\notin\gamma_k$, $k\in\gamma_k$, and otherwise $\gamma_k=\gamma$; $(k,l)\in\Lambda_\gamma$ is the forward bond of k (i.e., originated in the ket), and $s_{ki}=\pm 1$ comes from reordering the fermion operators. Relation (B5) is simplified using[12]

$$\det V(\gamma_k) s_{ki} = \det V(\gamma, i\to k), \tag{B6}$$

with

$$V(\gamma, i\to k)_{rp} = \begin{cases} v(k,j_p), & i_r = i, \\ V(\gamma)_{rp}, & \text{otherwise.} \end{cases} \tag{B7}$$

3. Matrix elements of the double-hopping terms

For $u_r>0\ \forall r$ we express $\langle \Delta_{kl}^\dagger \Delta_{ij}\rangle$, where Δ is given in Eq. (26). Here $\Delta_{kl}^\dagger$ creates a singlet bond. Δ_{ij} creates a pair of holes. With the results of Appendix , for $i\in A$, $j\in B$,

$$\Delta_{kl}^\dagger \Delta_{ij}(\gamma,\Lambda_\gamma) = \begin{cases} \dfrac{s}{2u_{kl}} \dfrac{\det V(\gamma_a)}{\det V(\gamma)} \left(\displaystyle\sum_{\substack{(r,n)\in\alpha(\gamma) \\ r\neq k}} \frac{u_{rj}u_{in}}{u_{rn}} + 2u_{ij} \right) & \text{if } (k,l)\in\alpha(\gamma), \\ & i\in\gamma \quad \text{if} \quad i\neq k, \\ & j\in\gamma \quad \text{if} \quad j\neq l, \\ 0, \quad \text{otherwise,} \end{cases} \tag{B8}$$

Where $s=-1$ if $i=k$ exclusive or $j=l$ and 1 otherwise; $V(\gamma_a)\equiv V(\gamma, i\to k, j\to l)$ is defined like Eq. (B7), with a possible replacement of a row *and* a column, and $\alpha(\gamma)$ is the set of forward bonds of A sublattice sites in $\Lambda(\gamma)$.

APPENDIX C: THE GUTZWILLER APPROXIMATION

The Gutzwiller approximation amounts to dropping the projector $\mathcal{P}(x)$ in definition (3) and setting $|\Psi[u,v;x]\rangle \to |\overline{\psi}[yu,zv]\rangle = |yu\rangle\otimes|zv\rangle$. The constants $y=y(u)$ and $z=z(v)$ are determined by the global constraint equations

$$\langle a_i^\dagger a_i\rangle = \langle b_i^\dagger b_i\rangle = (1-x)/2, \tag{C1}$$

$$\langle f_i^\dagger f_i\rangle = x, \tag{C2}$$

for y, z, respectively. In this section $\langle\cdots\rangle \equiv \langle\overline{\psi}|\cdots|\overline{\psi}\rangle/\langle\overline{\psi}|\overline{\psi}\rangle$.

$|yu\rangle$ is a Schwinger bosons mean field wave function,[15] on which we preform the Marshall transformation[15] $a_j\to -b_j$, $b_j\to a_j$, $j\in B$. Hence

$$|yu\rangle \to \exp\left(y\sum_{ij} u_{ij}(a_i^\dagger a_j^\dagger + b_i^\dagger b_j^\dagger)\right)|0\rangle. \tag{C3}$$

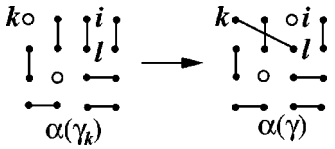

FIG. 16. The operator $f_i^\dagger f_k(a_k^\dagger a_i + b_k^\dagger b_i)$ turns a hole-pair configuration γ_k, $\alpha(\gamma_k)$ (left), with $k\in\gamma_k$, $(i,l)\in\alpha(\gamma_k)$, to the right configuration γ, $\alpha(\gamma)$ with $i\in\gamma$ and $(k,l)\in\alpha(\gamma)$. In $f_i^\dagger f_k(a_k^\dagger a_i + b_k^\dagger b_i)|\Psi\rangle$, this configuration has the coefficients u_{il} and $\det V(\gamma_k)$.

Operators are transformed accordingly, for example, $S_j^-\to -a_j^\dagger b_j$ for $j\in B$.

From Eqs. (C1) and (C2),

$$\langle S_i^+ S_i^- (1-f_i^\dagger f_i)^2\rangle = \langle n_i^a(1+n_i^b)\rangle\langle(1-n_i^f)^2\rangle = \frac{1-x}{2}\left(1+\frac{1-x}{2}\right)(1-x)^2, \tag{C4}$$

whereas $\langle\Psi|S_i^+S_i^-(1-f_i^\dagger f_i)^2|\Psi\rangle/\langle\Psi|\Psi\rangle = (1-x)/2$. Thus we use

$$(1-x/3)^{-1}\langle S_i^+ S_j^-\rangle \tag{C5}$$

as the GA for the long-range magnetic correlations and m_0 in the doped RVB state. *Empirically* we omit the $(1-x/3)^{-1}$ factor in the estimates of magnetic energy.

Using the extended Wick theorem,[21] for $i\in A$,

$$\langle S_i^+ S_j^-\rangle = \begin{cases} -\langle a_i^\dagger b_i a_j^\dagger b_j\rangle = -\langle a_i^\dagger a_j^\dagger\rangle\langle b_i b_j\rangle \equiv -\rho_{ij}^2, & j\in B, \\ \langle a_i^\dagger b_i b_j^\dagger a_j\rangle = \langle a_i^\dagger a_j\rangle\langle b_j^\dagger b_i\rangle + \delta_{ij}/2 \equiv \sigma_{ij}^2 + \delta_{ij}/2, & j\in A, \end{cases} \tag{C6}$$

where we used, for example, $\langle a_i^\dagger b_j\rangle = \langle a_i^\dagger b_j^\dagger\rangle = 0$.

Expanding $u_{\mathbf{k}} = \Sigma_j e^{i\mathbf{k}j} u_{0j}$, $\rho_{\mathbf{k}} = \Sigma_j e^{i\mathbf{k}j}\rho_{0j}$ and a similar expression for $\sigma_{\mathbf{k}}$,[21]

$$\rho_{\mathbf{k}} = \frac{y u_{\mathbf{k}}}{1-y^2 u_{\mathbf{k}}^2} \tag{C7}$$

and

$$\sigma_{\mathbf{k}} = \frac{y^2 u_{\mathbf{k}}^2}{1-y^2 u_{\mathbf{k}}^2}. \tag{C8}$$

The constraint equation (C1) becomes

$$\frac{y^2}{L^2}\sum_{\mathbf{k}}\frac{u_{\mathbf{k}}^2}{1-y^2u_{\mathbf{k}}^2}=\frac{1-x}{2}. \tag{C9}$$

We consider three cases.

1. Exponential bond amplitude

We calculate the spin-spin correlation function for

$$u(r)=\begin{cases}\exp(-r/\xi), & \mathbf{r}\ \text{bipartite},\\ 0, & \text{otherwise},\end{cases} \tag{C10}$$

with $\xi\gg 1$.

$$u_{\mathbf{k}}=\begin{cases}\int d^2\mathbf{r}\exp(-r/\xi)\exp(-i\mathbf{k}\cdot\mathbf{r})=2\pi\xi^{-1}/(k^2+\xi^{-2})^{3/2}, & \mathbf{k}\in\text{MBZ},\\ u_{\mathbf{k}}=-u_{\mathbf{k}-\boldsymbol{\pi}}, & \text{otherwise},\end{cases} \tag{C11}$$

where MBZ= magnetic Brillouin zone. Equation (C9) becomes

$$\frac{2y^2}{\xi^2}\int_{MBZ}\frac{d^2k}{(k^2+\xi^{-2})^3-(2\pi\xi^{-1}y)^2}=\frac{\pi y^2}{\xi^2}\int_{\xi^{-2}}^{\infty}\frac{dk}{k^3-(2\pi\xi^{-1}y)^2}=\frac{1-x}{2}, \tag{C12}$$

where we multiplied the left side in 2 to account for the integration over the complete Brillouin zone. In all our calculations we took the continuum limit (lattice constant$\to$0), where the upper bound of the integration $\to\infty$. This approximation works very well for slow decaying bond amplitude.[12]

Equation (C12) gives[22]

$$\frac{1}{3(2\pi)^{1/3}}\left(\frac{y}{\xi}\right)^{2/3}\times\left\{-\pi\sqrt{3}-2\sqrt{3}\arctan\left[\frac{1}{\sqrt{3}}\left(1+\left(\frac{2}{\pi^2y^2\xi^4}\right)^{1/3}\right)\right]+\ln\left[4\left(\frac{\pi y}{\xi}\right)^{4/3}+2\left(\frac{2\pi^2y^2}{\xi^8}\right)^{1/3}+\frac{2^{2/3}}{\xi^4}\right]-2\ln\left[\frac{2^{1/3}}{\xi^2}-2\left(\frac{\pi y}{\xi}\right)^{2/3}\right]\right\}=\frac{1-x}{2}. \tag{C13}$$

The argument of the last logarithm has to be sufficiently close to zero for Eq. (C13) to be satisfied. Therefore

$$2^{1/3}\xi^{-2}-2(\pi y\xi^{-1})^{2/3}\approx 0\Rightarrow y\approx\frac{1}{2\pi\xi^2}. \tag{C14}$$

Hence we can neglect on the left side of Eq. (C13) all terms but the last logarithm. Consequently,

$$y^2\cong\frac{1}{(2\pi)^2\xi^4}\left\{1-\frac{3\xi^2}{2^{1/3}}\exp\left[-(1-x)\frac{3\pi\xi^2}{2}\right]\right\}\equiv\frac{1}{(2\pi)^2\xi^4}\mathcal{D}. \tag{C15}$$

Equation (C6) becomes

$$\sigma_{\mathbf{r}}=2\int_{MBZ}d^2\mathbf{k}\sigma_{\mathbf{k}}\exp(i\mathbf{k}\cdot\mathbf{r})=\frac{\mathcal{D}}{2\pi\xi^6}\int dk\frac{kJ_0(kr)}{(\mathbf{k}^2+\xi^{-2})^3-\xi^{-6}\mathcal{D}}, \tag{C16}$$

where J_0 is the Bessel function.[22] Since the integrand in Eq. (C16) vanishes as $k\to 0$, we can replace J_0 with its approximation for $kr\gg 0$. Expanding the denominator to first order in k^2,

$$\sigma_{\mathbf{r}}\cong\frac{\mathcal{D}}{6\pi\sqrt{r\pi}\xi^2}\int_0^{\infty}dk\frac{\sqrt{k}}{k^2+a^2}[\cos(kr)+\sin(kr)]\equiv\frac{\mathcal{D}}{6\pi\sqrt{r\pi}\xi^2}Y_0, \tag{C17}$$

where $a^2=(1-\mathcal{D})/(3\xi^2)$. In the definition

$$Y_1\equiv\int_0^{\infty}dk\frac{\sqrt{k}}{k^2+a^2}\exp(ikr),$$

$Y_0=\mathrm{Re}\,Y_1+\mathrm{Im}\,Y_1$. Let us consider the integral

$$Y_2=\oint dz\frac{\sqrt{z}}{z^2+a^2}\exp(izr)=\int_{e^{i\pi}\infty}^{\infty}dk\frac{\sqrt{k}}{k^2+a^2}\exp(ikr),$$

where the close contour encircles the upper half of the complex plane. The part of the contour along the negative real axis is

$$\int_{e^{i\pi_\infty}}^{0} dk \frac{\sqrt{k}}{k^2+a^2}\exp(ikr) = i\int_0^\infty dk' \frac{\sqrt{k'}}{k'^2+a^2}\exp(-ik'r) = iY_1^\star,$$

where we substituted $k'=e^{-i\pi}k$. Hence $Y_2=Y_1+iY_1^\star=(1+i)(\mathrm{Re}\,Y_1+\mathrm{Im}\,Y_1)=(1+i)Y_0$. Using the residue method for Y_2,

$$\sigma_{\mathbf{r}} \propto \frac{\exp[-r\sqrt{(1-\mathcal{D})/(3\xi^2)}]}{\sqrt{r}}, \tag{C18}$$

and with Eq. (C15) we find for the correlation length of the spin-spin correlation function ξ_{ex}:

$$\xi_{ex} \approx \sqrt{\frac{3\xi^2}{4(1-\mathcal{D})}} = 2^{1/3}\exp\left[(1-x)\frac{3\pi}{2}\xi^2\right]. \tag{C19}$$

2. Gaussian bond amplitude

We calculate spin-spin correlation function for

$$u_{\mathbf{r}} = \begin{cases} \exp(-\mu r^2), & \mathbf{r} \text{ bipartite}, \\ 0, & \text{otherwise}. \end{cases}$$

For $\mathbf{k}\in$ MBZ,

$$u_{\mathbf{k}} = \frac{\pi}{\mu}\exp\left(-\frac{k^2}{4\mu}\right). \tag{C20}$$

Equation (C9) is

$$\frac{\mu}{2\pi}\int_0^1 \frac{dt}{\frac{\mu^2}{\pi^2 y^2}-t} = \frac{1-x}{4}, \tag{C21}$$

with the solution

$$y^2 = \frac{\mu^2}{\pi^2}\left\{1-\exp\left[-(1-x)\frac{\pi}{2\mu}\right]\right\} \equiv \frac{\mu^2}{\pi^2}\mathcal{G}. \tag{C22}$$

Calculation of $\sigma_{\mathbf{r}}$ is identical to the exponential case. Substituting in Eq. (C17) $a^2=2\mu(1-\mathcal{G})$,

$$\sigma_{\mathbf{r}} \propto \frac{\exp[-r\sqrt{2\mu(1-\mathcal{G})}]}{\sqrt{r}}, \tag{C23}$$

and hence the spin-spin correlation function decays exponentially with correlation length:

$$\xi_g = \frac{1}{\sqrt{8\mu(1-\mathcal{G})}} = \frac{1}{\sqrt{8\mu}}\exp\left[(1-x)\frac{\pi}{4\mu}\right]. \tag{C24}$$

3. Power law bond amplitude

For the bond amplitude

$$u_{\mathbf{r}} = \begin{cases} \dfrac{\epsilon^3}{(r^2+\epsilon^2)^{3/2}}, & \mathbf{r} \text{ bipartite}, \\ 0, & \text{otherwise}, \end{cases} \tag{C25}$$

we show, in the continuum limit, that for $0<\epsilon<\epsilon_0$, $S(\pi,\pi)$ is finite and hence $m_0=0$.

Calculations of the GA on lattices of size $L\leqslant 512$ show that for any ϵ, the spin-spin correlation function calculated with function (C25) decays slower than with $u=1/r^3$. This suggests that $m_0=0$ for $u=1/r^3$.

$$S(\pi,\pi) = \sum_j |\langle S^+_{\mathbf{r}_j} S^-_0\rangle| = \sum_j \sigma^2_{\mathbf{r}_j} + \rho^2_{\mathbf{r}_j} + \frac{1}{2} = \frac{1}{L^2}\sum_{\mathbf{q}} (\sigma^2_{\mathbf{q}}+\rho^2_{\mathbf{q}}) + \frac{1}{2},$$

where we used Eq. (C6). For $\mathbf{k}\in$ MBZ,[22]

$$u_{\mathbf{k}} = 2\pi\epsilon^2 e^{-\epsilon k}. \tag{C26}$$

From Eqs. (C7) and (C8), $\rho_{\mathbf{k}} \overset{k\to\infty}{\to} e^{-\epsilon k}$ and $\sigma_{\mathbf{k}} \overset{k\to\infty}{\to} e^{-2\epsilon k}$. Hence $S(\pi,\pi)$ might diverge only if there is k_0 such that $(1-ae^{-2\epsilon k})_{k=k_0}=0$, where $a=a(\epsilon)=(2\pi y\epsilon^2)^2$. Therefore, if $a<1$, $S(\pi,\pi)$ is finite.

Equation (C9) for y is

$$\frac{a}{\pi}\int_0^\infty dk \frac{ke^{-2\epsilon k}}{1-ae^{-2\epsilon k}} = \frac{a}{\pi}\int_0^\infty dk \frac{k}{e^{2\epsilon k}-a} = \frac{1-x}{2}, \tag{C27}$$

which becomes[22]

$$\sum_{p=1}^{\infty}\frac{a^p}{p^2} = \pi\epsilon^2(1-x). \tag{C28}$$

The right side of Eq. (C28) is y independent, and increases with ϵ; hence a increases with ϵ. Therefore $a(\epsilon_0)=1$. For $a=1$, the left side of Eq. (C28) is $\pi^2/6$ and

$$\epsilon_0 = \sqrt{\frac{\pi}{6(1-x)}}, \tag{C29}$$

and for $\epsilon<\epsilon_0$, $S(\pi,\pi)$ is finite and hence $m_0=0$.[23]

*Present address: Compugen Ltd., 72 Pinhas Rosen St., Tel Aviv, Israel. Electronic address: moshe@compugen.co.il

†Electronic address: assa@pharaoh.technion.ac.il

[1] Ch. Neidermayer *et al.*, Phys. Rev. Lett. **80**, 3843 (1998).

[2] S. Wakimoto, K. Yamada, S. Ueki, G. Shirane, Y. S. Lee, M. A. Kastner, K. Hirota, P. M. Gehring, Y. Endoh, and R. J. Birgeneau, cond-mat/9902319 (unpublished).

[3] K. Yamada *et al.*, Phys. Rev. B **57**, 6165 (1998); H. A. Mook *et al.*, Nature (London) **395**, 580 (1998); Y. S. Lee *et al.*, cond-mat/9902157 (unpublished).

[4] M. Inui, S. Doniach, and M. Gabay, Phys. Rev. B **38**, 6631 (1988); B. I. Shraiman and E. D. Siggia, Phys. Rev. Lett. **62**, 1564 (1989); V. Cherepanov, I. Ya. Korenblit, Amnon Aharony, O. Entin-Wohlman, cond-mat/9808235 (unpublished).

[5] P. W. Anderson, Science **235**, 1196 (1987).
[6] W. Marshall, Proc. R. Soc. London, Ser. A **232**, 48 (1955); E. Lieb and D. C. Mattis, J. Math. Phys. **3**, 749 (1962).
[7] S. Liang, B. Doucot, and P. W. Anderson, Phys. Rev. Lett. **61**, 365 (1988).
[8] T. Miyazaki, D. Yoshioka, and M. Ogata, Phys. Rev. B **51**, 2966 (1995).
[9] V. J. Emery and S. A. Kivelson, Nature (London) **374**, 434 (1995).
[10] Bill Sutherland, Phys. Rev. B **37**, 3786 (1988); M. Kohmoto and Y. Shapir, *ibid.* **37**, 9439 (1988).
[11] *Applications of the Monte Carlo Method in Statistical Physics*, edited by K. Binder (Springer-Verlag, Berlin, 1984).
[12] M. Havilio, Ph.D. thesis, Technion, 1999.
[13] D. Ceperley, G. V. Chester, and M. H. Kalos, Phys. Rev. B **16**, 3081 (1977).
[14] M. Havilio, Phys. Rev. B **54**, 11 929 (1996).
[15] A. Auerbach, *Interacting Electrons and Quantum Magnetism* (Springer-Verlag, New York, 1994).
[16] N. E. Bonesteel and W. Wilkins, Phys. Rev. Lett. **66**, 1232 (1991).
[17] A. W. Sandvik, Phys. Rev. B **56**, 11 678 (1997).
[18] C. L. Kane *et al.*, Phys. Rev. B **41**, 2653 (1990); A. Auerbach, *ibid.* **48**, 3287 (1993).
[19] E. Dagotto, Rev. Mod. Phys. **66**, 763 (1994).
[20] Pair hopping terms with *weak* Hubbard interactions can drive superconductivity even at half filling, as shown by F. F. Assaad, M. Imada, and D. J. Scalapino, Phys. Rev. Lett. **77**, 4592 (1996); S-C. Zhang, Science **275**, 1089 (1997). Here we treat the large-U system.
[21] M. Raykin and A. Auerbach, Phys. Rev. B **47**, 5118 (1993).
[22] I. S. Gradsteyn and I. M. Ryzhik, *Table of Integrals, Series and Products* (Academic Press, New York, 1980) .
[23] For simplicity, we ignore frustration and limit $\Psi[u,v]$ to have purely antiferromagnetic correlations and uniform charge distributions. Although experiments observe small doping-dependent shifts in ordering wave vectors (stripes), these effects should be small on the quantum fluctuations of the *local* magnetization.